

Constraining the Bestest Little Higgs model with recent results from the LHC

Pat Kalyniak,^a Travis A. W. Martin,^b Kenneth Moats^a

^a*Ottawa-Carleton Institute for Physics, Department of Physics, Carleton University
Ottawa, Canada K1S 5B6*

^b*TRIUMF, 4004 Wesbrook Mall, Vancouver, Canada V6T 2A3*

E-mail: kalyniak@physics.carleton.ca, tmartin@triumf.ca,
kmoats@physics.carleton.ca

ABSTRACT: In this paper, we use the latest Higgs results from ATLAS and CMS to constrain the parameter space of the Bestest Little Higgs model. We account for all production and decay modes explored at ATLAS and CMS, in two scenarios: a general case, which assumes the h_0 state is light ($m_{h_0} \approx 125$ GeV) and the masses of the other states (H_0 and A_0) vary within the allowed mass parameter range, and a case with a near-degeneracy between the masses of the h_0 , A_0 and, for some choices of parameters, the H_0 fields. We show that the general case provides large regions of parameter space that are in agreement with the CMS results ($\mu_{\gamma\gamma} \approx 1$ and $\mu_{WW} \approx \mu_{ZZ} \approx 1$), but little parameter space that is in agreement with the ATLAS results ($\mu_{\gamma\gamma} > 1$ and $\mu_{WW} \approx 1$). We also show that the unexpected ATLAS results can be accounted for within the near-degenerate scenario we explored, when we exclude the $\mu_{WW} \neq \mu_{ZZ} > 1$ result. More accurate measurements, including the $b\bar{b}$, $\tau^+\tau^-$ and $Z\gamma$ final states, with higher luminosity will be crucial to determining the status of the BLH model.

Contents

1	Introduction	1
2	Calculations	3
2.1	Production and Decay	3
3	Model Details and Couplings	8
3.1	Scalar Sector	8
3.2	Gauge Sector	11
3.3	Fermion Sector	12
3.4	Parameter Survey	13
4	Results	15
5	Summary	17

1 Introduction

After analyzing the results from approximately 5 fb^{-1} of integrated luminosity at both 7 TeV and 8 TeV centre-of-mass collision energies, both ATLAS and CMS revealed the discovery of a new resonance in the $\gamma\gamma$, $ZZ^* \rightarrow 4l$ and $WW^* \rightarrow l^+l^- \cancel{E}_T$ decay channels, consistent with the Standard Model (SM) Higgs boson at a mass of approximately 125 GeV, with a combined significance of more than 5σ [1, 2]. Now that the remaining 8 TeV collision data, corresponding to approximately 20 fb^{-1} of integrated luminosity, has been analyzed, this new state continues to be consistent with the SM Higgs boson. Assuming that this is, in fact, a Higgs boson, there are indications that its branching ratios might deviate from those of the SM Higgs boson, particularly in the diphoton decay rate that is sensitive to the presence of new physics [3, 4]. More data will be needed for precise determination of the branching ratios.

Prior to Moriond 2013, both the CMS and the ATLAS experiments found an enhancement in the diphoton signal strength, without significant deviations from SM values in the ZZ^* and WW^* signal strengths [3, 5–11]. Following Moriond 2013, CMS updated their diphoton analysis with results that were in better agreement with the SM predictions [12]. Of interest, however, is that ATLAS [13, 14] still observes an excess in the diphoton rate at a significance of approximately 2σ ; and the diphoton resonance provides a best fit invariant mass for the Higgs boson that is larger than the measured resonance mass for the ZZ^* final state (126.8 GeV versus 124.3 GeV).

These results have a significant impact on studies of beyond the Standard Model physics, as many models are motivated by explanations for Higgs phenomena and thus

predict results that differ from those expected for a SM Higgs boson. Thus, there may be significant constraints placed on such models by comparing both the measured mass of the Higgs-like state and the measured signal strengths ($\hat{\mu}$) for each final state to the predicted values from the model. In general, vector boson fusion (VBF), vector boson associated production (VH), and the ZZ^*/WW^* decay modes are sensitive to modifications of the Higgs boson couplings to gauge bosons; top quark associated production (ttH) and the fermion decay modes are sensitive to modifications of the Higgs boson couplings to fermions; and gluon fusion (ggF) and the diphoton ($\gamma\gamma$) and $Z\gamma$ loop-induced decay modes are sensitive to the presence of new coloured and electrically charged states, respectively, that couple to the Higgs boson, as well as modifications to the hW^+W^- and $ht\bar{t}$ couplings.

In general, Little Higgs models are more highly constrained by precision electroweak measurements than by the LHC Higgs results [15, 16]. A recent model, the Bestest Little Higgs (BLH) model [17], alleviates these constraints due to the presence of a custodial symmetry and a disassociation of the masses of the top partner and heavy gauge boson states. The BLH model features a global $SO(6)_A \times SO(6)_B$ symmetry that is broken to a diagonal $SO(6)_V$ at a scale $f \sim \mathcal{O}(\text{TeV})$ when the non-linear sigma field, Σ , develops a vev ($\langle \Sigma \rangle = \mathbb{1}$). The resulting 15 pseudo-Nambu Goldstone bosons are parameterized as two real triplets, ϕ^a and η^a ($a = 1, 2, 3$), two complex Higgs doublets, h_1 and h_2 , and a real singlet σ . A general two Higgs doublet potential is generated in part explicitly and in part radiatively, where the quartic coupling for the Higgs arises when integrating out the heavy scalar singlet, σ . A second global symmetry of the form $SU(2)_C \times SU(2)_D$ is also present, which is broken to a diagonal $SU(2)$ at a scale $F > f$. Both of these global symmetries are gauged by the same $SU(2)_A \times SU(2)_B$ gauge bosons, while the $SO(6)_A \times SO(6)_B$ symmetry is also gauged by the hypercharge $U(1)_Y$. This leads to an extra heavy gauge boson triplet (W'^{\pm}, Z') with masses proportional to $f^2 + F^2$, which reduces their contribution to precision electroweak observables. Fermions in the BLH model, including the newly introduced top partners ($T, B, T_b^{2/3}, T_b^{5/3}, T_5$ and T_6), only transform under the global $SO(6)_A \times SO(6)_B$. This leads to the top partners being lighter than the heavy gauge bosons, and results in a lesser degree of fine tuning than in other Little Higgs models.

The BLH model has a large parameter space, allowing for a wide range of experimental signatures that could potentially reproduce either the CMS or the ATLAS results. Since the BLH model is a Type I two Higgs doublet model (2HDM), it also presents the possibility for a near degeneracy between two or three physical scalar fields (h_0, H_0 and A_0), which can result in an enhancement in the diphoton rate without affecting the ZZ^* or WW^* rates, similar to what has been observed at ATLAS. Furthermore, near-degeneracy could also explain the observed difference in the diphoton and ZZ^* invariant mass peaks. Type I 2HDM models are not as strongly affected by meson factory constraints as type II 2HDM models [18], and so the near-degenerate case presents a very interesting possibility that we explore in this paper.

In this paper, we explore the Higgs results in the Bestest Little Higgs model, accounting for all production and decay modes explored at ATLAS and CMS, in two scenarios: a general case, which assumes the h_0 state is light (≈ 125 GeV) and the other states (H_0 and A_0) vary within the allowed mass parameter range, and a second case with a near-

degeneracy between the masses of the h_0 and A_0 fields. The masses of the h_0 and A_0 fields are input parameters for the model, while the H_0 mass depends on other parameters and may or may not be similarly near-degenerate in the latter scenario. In Sec. 2, we describe the formalism we use in our calculations of the Higgs results, while in Sec. 3 we describe the details of the BLH model that are relevant to our calculations. In Sec. 4, we compare the BLH model predictions to the measured results from ATLAS and CMS in both scenarios.

2 Calculations

2.1 Production and Decay

As shown in [19–21], the scalar interactions of a Little Higgs model Lagrangian can be normalized to the form of the SM expressions by introducing scaling factors y_i , such that

$$\mathcal{L}_h = - \sum_f C_{S_0 \bar{f} f} S_0 \bar{f} f + \sum_V C_{S_0 V V} S_0 V^\dagger V - \sum_S C_{S_0 S S} S_0 S^\dagger S \quad (2.1)$$

$$= - \sum_f \frac{m_f}{v} y_{S_0 \bar{f} f} S_0 \bar{f} f + \sum_V 2 \frac{M_V^2}{v} y_{S_0 V V} S_0 V^\dagger V - \sum_S 2 \frac{M_S^2}{v} y_{S_0 S S} S_0 S^\dagger S \quad (2.2)$$

for fermion species f , vector bosons V and scalars S . The S_0 label denotes the h_0 , H_0 , and A_0 (with an appropriate γ_5 factor) for the fermion interactions, and the h_0 and H_0 for the vector boson and scalar boson interaction terms. The parameters (v, M_i, C_i, y_i) are model dependent. The expression for the vev, v , will be discussed further in Sec. 3.

A Higgs boson of approximately 125 GeV decays predominantly to pair produced, kinematically accessible states, such as $b\bar{b}$ and $\tau^+\tau^-$, and to one on-shell and one off-shell vector boson (ZZ^* and WW^*). Decays to diphotons, digluons and $Z\gamma$ are also possible through loop interactions [19]. In the BLH model, all three physical Higgs states (h_0 , H_0 and A_0) can decay to light fermions and to loop-induced final states, but only the CP-even states (h_0 and H_0) can decay to pairs of gauge bosons, as shown in Figures 1, 2 and 3. In our calculations, we account for the contributions from all three Higgs states, and include all new particle states of the model that contribute to the loop diagrams.

When the scalar couplings are expressed in the form of Eq. 2.2, the partial decay widths of the $S_0 = h_0, A_0, H_0$ can be written in terms of the SM calculated values (we use the values calculated in [22]) multiplied by some combination of scaling factors. For direct decays, this is straight forward, however for loop-induced decays the scaling factors must also include the loop factors. The direct decays are given by

$$\begin{aligned} \Gamma(S_0 \rightarrow b\bar{b})_{BLH} &= \left(\frac{y_{S_0 b\bar{b}}}{y_v} \right)^2 \Gamma(S_0 \rightarrow b\bar{b})_{SM} && \equiv r_{S_0 b\bar{b}} \Gamma(S_0 \rightarrow b\bar{b})_{SM} \quad (2.3) \\ \Gamma(S_0 \rightarrow c\bar{c})_{BLH} &= \left(\frac{y_{S_0 c\bar{c}}}{y_v} \right)^2 \Gamma(S_0 \rightarrow c\bar{c})_{SM} && \equiv r_{S_0 c\bar{c}} \Gamma(S_0 \rightarrow c\bar{c})_{SM} \\ \Gamma(S_0 \rightarrow \tau^+\tau^-)_{BLH} &= \left(\frac{y_{S_0 \tau\tau}}{y_v} \right)^2 \Gamma(S_0 \rightarrow \tau^+\tau^-)_{SM} && \equiv r_{S_0 \tau\tau} \Gamma(S_0 \rightarrow \tau^+\tau^-)_{SM} \\ \Gamma(S_0 \rightarrow ZZ^*)_{BLH} &= \left(\frac{y_{S_0 ZZ} y_{Z\bar{f}f}^2}{y_v} \right)^2 \Gamma(S_0 \rightarrow ZZ^*)_{SM} && \equiv r_{S_0 ZZ} \Gamma(S_0 \rightarrow ZZ^*)_{SM} \end{aligned}$$

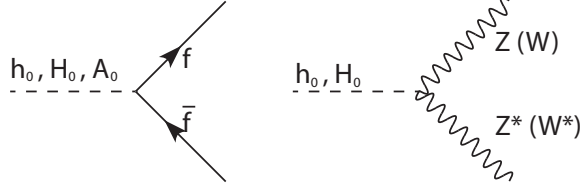


Figure 1. Direct decay modes of the h_0 , H_0 and A_0 states.

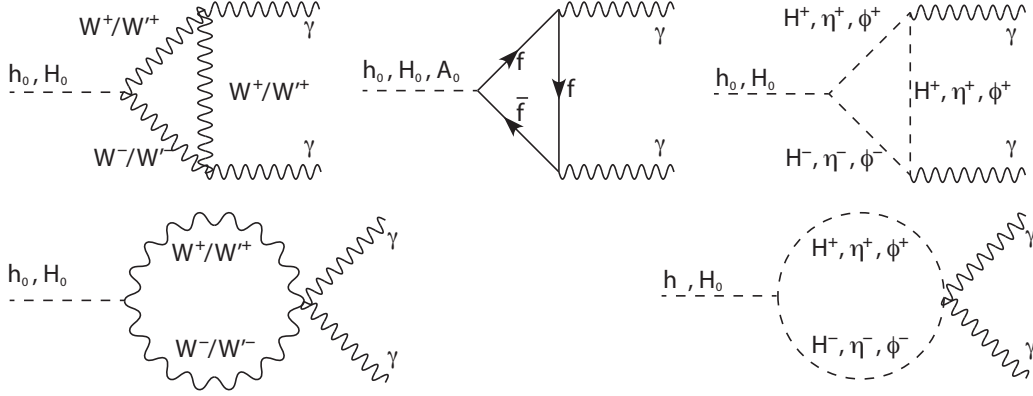


Figure 2. Loop diagrams contributing to decays to pairs of photons, where f refers to all fermions with an electric charge, including heavy, vector-like quark states. Similar diagrams exist for the $Z\gamma$ final state, where one of the photons is replaced by a Z boson.

$$\Gamma(S_0 \rightarrow WW^*)_{BLH} = \left(\frac{y_{S_0 WW} y_{W\bar{f}f}^2 y_{M_W}}{y_v} \right)^2 \Gamma(S_0 \rightarrow WW^*)_{SM} \equiv r_{S_0 WW} \Gamma(S_0 \rightarrow WW^*)_{SM}$$

where the factors of y_v account for the differences between the vev in the BLH model and the SM vev, such that $v_{BLH} = y_v v_{SM}$, and are discussed in further detail in the following section. The factor $y_{M_W} \equiv M_W^{BLH}/M_W^{SM}$ is the ratio of the W boson mass calculated in the BLH model and in the SM, and appears when making the replacement $g = 2M_W/v$ in the expression for the $S_0 \rightarrow WW^*$ partial width [23]. The factors of $y_{V\bar{f}f}$ are given by $y_{W\bar{f}f} = (g_{W\bar{f}f}^L)_{BLH}/(g_{W\bar{f}f}^L)_{SM}$ and $y_{Z\bar{f}f} = \sqrt{((g_{Z\bar{f}f}^{BLH})_L^2 + (g_{Z\bar{f}f}^{BLH})_R^2)/((g_{Z\bar{f}f}^{SM})_L^2 + (g_{Z\bar{f}f}^{SM})_R^2)}$, and account for differences in the expressions of the couplings of the light vector bosons to fermions in the BLH model. We include $Z \rightarrow l^+l^-$ and $W^\pm \rightarrow l^\pm\nu_l$ decays ($l = e, \mu$) in the calculation of the ZZ^* and WW^* decay widths, as dictated by the experimental results from ATLAS and CMS [3, 5–11]. In light of recent ATLAS and CMS results in the $Z\gamma$ channel [24, 25], the $Z \rightarrow l^+l^-$ decay ($l = e, \mu$) is also taken into account in this channel by including a factor of $y_{Z\bar{f}f}^2$ in the expression for $\Gamma(S_0 \rightarrow Z\gamma)$ below.

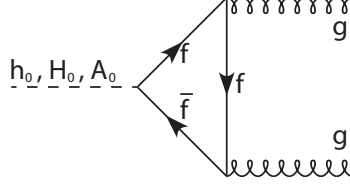


Figure 3. Loop diagrams contributing to decays to pairs of gluons, where f refers to all fermions with an color charge, including heavy, vector-like quark states. This is also the process for the gluon-fusion production mode.

The expressions for the partial widths of the loop-induced decay modes are given by

$$\begin{aligned}
\Gamma(S_0 \rightarrow \gamma\gamma) &= \frac{\left| \sum_{f_{SM}} A_{f,\gamma\gamma}^{BLH} + A_{W,\gamma\gamma}^{BLH} + A_{new,\gamma\gamma}^{BLH} \right|^2}{y_v^2 \left| \sum_{f_{SM}} A_{f,\gamma\gamma}^{SM} + A_{W,\gamma\gamma}^{SM} \right|^2} \Gamma(S_0 \rightarrow \gamma\gamma)_{SM} \\
&\equiv r_{S_0\gamma\gamma} \Gamma(S_0 \rightarrow \gamma\gamma)_{SM} \\
\Gamma(S_0 \rightarrow Z\gamma) &= \frac{\left| \sum_{f_{SM}} A_{f,Z\gamma}^{BLH} + A_{W,Z\gamma}^{BLH} + A_{new,Z\gamma}^{BLH} \right|^2}{y_v^2 \left| \sum_{f_{SM}} A_{f,Z\gamma}^{SM} + A_{W,Z\gamma}^{SM} \right|^2} y_{Zff}^2 \Gamma(S_0 \rightarrow Z\gamma)_{SM} \\
&\equiv r_{S_0Z\gamma} \Gamma(S_0 \rightarrow Z\gamma)_{SM} \\
\Gamma(S_0 \rightarrow gg) &= \frac{\left| \sum_{q_{SM}} A_{q,gg}^{BLH} + A_{new,gg}^{BLH} \right|^2}{y_v^2 \left| \sum_{q_{SM}} A_{q,gg}^{SM} \right|^2} \Gamma(S_0 \rightarrow gg)_{SM} \\
&\equiv r_{S_0gg} \Gamma(S_0 \rightarrow gg)_{SM}
\end{aligned} \tag{2.4}$$

In this form, the A_{new}^{BLH} terms in each channel account for the contributions from loops involving only the new (non-SM) particles of the BLH model. Thus, we find the expressions

$$\begin{aligned}
A_{new,\gamma\gamma}^{BLH} &= \sum_f A_{f,\gamma\gamma}^{BLH} + A_{W',\gamma\gamma}^{BLH} + \sum_S A_{S,\gamma\gamma}^{BLH} \\
A_{new,Z\gamma}^{BLH} &= 2 \sum_f A_{f,Z\gamma}^{BLH} + A_{W',Z\gamma}^{BLH} + 2 \sum_S A_{S,Z\gamma}^{BLH} \\
A_{new,gg}^{BLH} &= \sum_f A_{f,gg}^{BLH}.
\end{aligned} \tag{2.5}$$

The expressions for the A terms in the BLH model are given by:

$$\begin{aligned}
A_{f,\gamma\gamma}^{BLH} &\equiv N_c^f y_{S_0\bar{f}f} Q_f^2 F_f(\tau_f) \\
A_{V,\gamma\gamma}^{BLH} &\equiv y_{S_0VV} Q_V F_V(\tau_V) \\
A_{S,\gamma\gamma}^{BLH} &\equiv y_{S_0SS} Q_S^2 F_S(\tau_S) \\
A_{f,Z\gamma}^{BLH} &\equiv N_c^f y_{S_0\bar{f}f} \left[\left(g_{Z\bar{f}f}^{BLH} \right)_L + \left(g_{Z\bar{f}f}^{BLH} \right)_R \right] Q_f F_f(\tau_f, \lambda_f) \\
A_{V,Z\gamma}^{BLH} &\equiv y_{S_0VV} g_{ZVV}^{BLH} Q_V F_V(\tau_V, \lambda_V) \\
A_{S,Z\gamma}^{BLH} &\equiv y_{S_0SS} g_{ZSS}^{BLH} Q_S F_S(\tau_S, \lambda_S) \\
A_{f,gg}^{BLH} &\equiv y_{S_0\bar{f}f} F_f(\tau_f), \tag{2.6}
\end{aligned}$$

where the SM expressions from the denominators in Eq. 2.4 can be found by setting the y scaling factors in Eq. 2.6 to unity. In these expressions, Q is the electric charge of the particle, and N_c is the number of colours (3 for quarks, 1 for leptons). The form factors $F_f(\tau_f)$, $F_V(\tau_V)$ and $F_S(\tau_S)$ (and similarly for $F_f(\tau_f, \lambda_f)$, $F_V(\tau_V, \lambda_V)$ and $F_S(\tau_S, \lambda_S)$) are solved by integrating over the fermion (f), gauge boson (V) and scalar (S) loops, respectively. These are given by:

$$\begin{aligned}
F_f(\tau) &= -2\tau(1 + (1 - \tau)f(\tau)) \\
F_V(\tau) &= 2 + 3\tau + 3\tau(2 - \tau)f(\tau) \\
F_S(\tau) &= \tau(1 - \tau f(\tau)) \\
F_f(\tau, \lambda) &= I_1(\tau, \lambda) - I_2(\tau, \lambda) \\
F_V(\tau, \lambda) &= 4(3 - \tan^2 \theta_w)I_2(\tau, \lambda) \\
&\quad + ((1 + 2\tau^{-1})\tan^2 \theta_w - 5 - 2\tau^{-1})I_1(\tau, \lambda) \\
F_S(\tau, \lambda) &= -I_1(\tau, \lambda) \tag{2.7}
\end{aligned}$$

where

$$\begin{aligned}
I_1(x, y) &= \frac{xy}{2(x-y)} + \frac{x^2y^2}{2(x-y)^2}(f(x) - f(y)) + \frac{x^2y}{(x-y)^2}(g(x) - g(y)) \\
I_2(x, y) &= -\frac{xy}{2(x-y)}(f(x) - f(y)) \\
f(x) &= \begin{cases} [\arcsin(1/\sqrt{x})]^2, & x \geq 1 \\ -\frac{1}{4} \left[\ln \left(\frac{1 + \sqrt{1-x}}{1 - \sqrt{1-x}} \right) - i\pi \right]^2, & x < 1 \end{cases}
\end{aligned}$$

$$g(x) = \begin{cases} \sqrt{x-1} \arcsin(1/\sqrt{x}), & x \geq 1 \\ \frac{\sqrt{1-x}}{2} \left[\ln \left(\frac{1+\sqrt{1-x}}{1-\sqrt{1-x}} \right) - i\pi \right], & x < 1 \end{cases} \quad (2.8)$$

In the above, $\tau_{f,V,S} \equiv 4m_{f,V,S}^2/m_{S_0}^2$ and $\lambda_{f,V,S} \equiv 4m_{f,V,S}^2/m_Z^2$, for field f , V or S , with corresponding mass $m_{f,V,S}$. In the limit that $\tau_i \gg 1$, these factors approach the values of $F_f \rightarrow -4/3$, $F_V \rightarrow 7$, and $F_S \rightarrow -1/3$.

For new fields whose masses are proportional to f or F , such as the new vector-like quarks and heavy gauge bosons in the BLH model, the scaling factors behave as $y_i \propto (v/f)^k$, where $k \geq 1$. Thus, while the factor of $F_i(\tau)$ may increase in magnitude with increasing mass of the new state, the scaling factor, y_i , decreases at a faster rate, and very high mass states typically have only a small contribution to the loop factors. It is also possible that loops involving both W^\pm and W'^\pm or ϕ^\pm and η^\pm contribute to the $S_0 \rightarrow \gamma\gamma$ and $S_0 \rightarrow Z\gamma$ decay widths due to vertices of the form of $hW^+W'^-$ and $h\phi^+\eta^-$. However, since the $\gamma W^+W'^-$ and $\gamma\phi^+\eta^-$ couplings of the BLH model are suppressed at $\mathcal{O}(v^2/f^2)$, these mixed loops can be safely neglected in this model.

Expressions similar to those for the decay modes exist for the production modes. At the LHC, the primary production mode is through gluon-gluon fusion (ggF), which occurs via the reverse of the diagram in Figure 3. The other production mechanisms at the LHC include vector boson fusion (VBF), associated production with a vector boson (VH), and associated production with top quarks (ttH). The diagrams for these sub-dominant processes are given in Fig. 4.

In the BLH model, the production modes are modified from the SM expressions in a similar manner as the decay modes, and can be expressed as a multiplicative factor times the SM values, such as:

$$\begin{aligned} \sigma(ggF)_{BLH} &= r_{S_0gg} \sigma(ggF)_{SM} \\ \sigma(VBF)_{BLH} &= (y_{S_0WW}^2 y_{M_W}^2 / y_v^2) \sigma(VBF)_{SM} \\ \sigma(WH)_{BLH} &= (y_{S_0WW}^2 y_{M_W}^2 / y_v^2) \sigma(WH)_{SM} \\ \sigma(ZH)_{BLH} &= (y_{S_0ZZ}^2 / y_v^2) \sigma(ZH)_{SM} \\ \sigma(VH)_{BLH} &= \sigma(WH)_{BLH} + \sigma(ZH)_{BLH} \\ \sigma(ttH)_{BLH} &= y_{S_0t\bar{t}}^2 \sigma(ttH)_{SM} \end{aligned} \quad (2.9)$$

The factor modifying the gluon fusion production mode, r_{S_0gg} , is the same as for the gg decay mode, given in Eq. 2.4. Since $y_{M_W} \approx 1$ and $y_{S_0WW} = y_{S_0ZZ}$ in the BLH model due to custodial symmetry, the VBF and VH expressions are essentially independent of whether the gauge boson is a Z or a W .

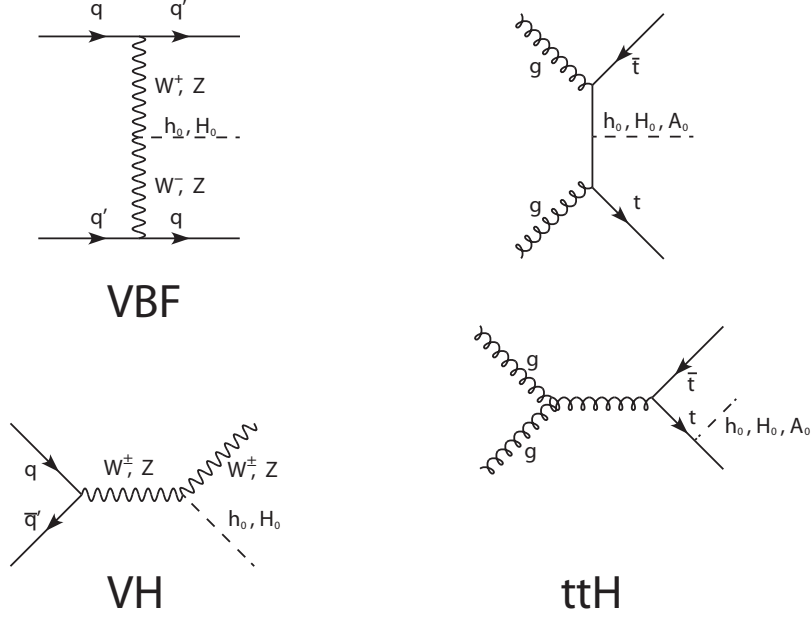


Figure 4. Subdominant production modes for Higgs bosons at the LHC - vector boson fusion (VBF), associated production with a vector boson (VH), and associated production with top quarks (ttH).

3 Model Details and Couplings

The $SO(6)_A \times SO(6)_B \rightarrow SO(6)_V$ Bestest Little Higgs (BLH) model [17] is a non-linear sigma model with two non-linear sigma fields, Σ and Δ , with respective symmetry breaking scales f and F , which are on the order of the TeV scale and satisfy the relation $F > f$. In addition to the four new Higgs states common to 2HDMs (H_0 , A_0 , and H^\pm), the BLH model includes six new heavy quarks (T , B , T_5 , T_6 , $T_b^{2/3}$, and $T_b^{5/3}$), three new gauge bosons (Z' and W'^\pm), two scalar triplets (η_0 , η^\pm , ϕ_0 , and ϕ^\pm) and one scalar singlet (σ). The following subsections deal with the determination of the scaling factors, y_i , for all states in the BLH model.

3.1 Scalar Sector

The BLH model Higgs fields, h_1 and h_2 , form a two Higgs doublet potential that undergoes spontaneous symmetry breaking. The most basic form of this potential is given below as in [17], and is sufficient to understand EWSB in the model:

$$V = \frac{1}{2}m_1^2 h_1^T h_1 + \frac{1}{2}m_2^2 h_2^T h_2 - B_\mu h_1^T h_2 + \frac{\lambda_0}{2}(h_1^T h_2)^2. \quad (3.1)$$

In this form, each of the Higgs “doublets” are written as $\mathbf{4}$'s of $SO(4)$, which have the same degrees of freedom and hypercharge values as the standard two Higgs doublets from [26]. Additionally, while there are other quartic terms present in the BLH model (namely $(h_1^T h_1)^2$, $(h_2^T h_2)^2$, $(h_1^T h_1)(h_2^T h_2)$, and $(h_1^T h_1 + h_2^T h_2)(h_1^T h_2)$), their coefficients are generated

at loop level and do not significantly affect the details of electroweak symmetry breaking. As these terms have a small effect on the diagonalization, they are ignored in the determination of the mass eigenstates. They are not ignored in the determination of the couplings, however, as they comprise the dominant contribution to the interactions of the scalar triplets with the Higgs fields.

The parameters in this potential are generated in part explicitly and in part radiatively, as with other Little Higgs models, and spontaneous symmetry breaking occurs for parameter values that satisfy $B_\mu > m_1 m_2$. The minimization condition is achieved by shifting the first component of each of h_1 and h_2 by a respective vacuum expectation value (vev), v_1 and v_2 . These vevs can be parameterized by a mixing angle, such that $v_1 = v \sin \beta$ and $v_2 = v \cos \beta$, where v is related to the Standard Model vev via the relation $v = y_v v_{SM}$ (the expression for y_v will be addressed in the next subsection).

Diagonalizing the mass matrix for the scalar sector results in three physical neutral scalar fields (h_0 , H_0 and A_0 , along with the unphysical G_0), and two physical charged scalar fields (H^\pm , along with the unphysical G^\pm), such that

$$\begin{aligned}
h_1[1] &= \cos \alpha h_0 - \sin \alpha H_0 + v \sin \beta \\
h_2[1] &= \sin \alpha h_0 + \cos \alpha H_0 + v \cos \beta \\
h_1[2] &= -\cos \beta A_0 + \sin \beta G_0 \\
h_2[2] &= +\sin \beta A_0 + \cos \beta G_0 \\
h_1^\pm &= -\cos \beta H^\pm + \sin \beta G^\pm \\
h_2^\pm &= +\sin \beta H^\pm + \cos \beta G^\pm.
\end{aligned} \tag{3.2}$$

The four parameters in the Higgs potential (m_1 , m_2 , B_μ and λ_0) can be re-parameterized in a more phenomenological fashion in terms of the masses of the h_0 and A_0 states, as well as the mixing angle β and the vev, $v = \sqrt{v_1^2 + v_2^2}$. In this parameterization, we find the following expressions:

$$\begin{aligned}
\lambda_0 &= \frac{m_{h_0}^2}{v^2} \left(\frac{m_{h_0}^2 - m_{A_0}^2}{m_{h_0}^2 - \sin^2(2\beta)m_{A_0}^2} \right) \\
B_\mu &= \frac{1}{2}(m_{A_0}^2 + v^2 \lambda_0) \sin(2\beta) \\
\tan \alpha &= \frac{B_\mu \cot(2\beta) + \sqrt{B_\mu^2 / \sin^2(2\beta) - 2\lambda_0 B_\mu v^2 \sin(2\beta) + \lambda_0^2 v^4 \sin^2(2\beta)}}{B_\mu - \lambda_0 v^2 \sin(2\beta)} \\
m_{H^\pm}^2 &= m_{A_0}^2 \\
m_{H_0}^2 &= \frac{B_\mu}{\sin(2\beta)} + \sqrt{\frac{B_\mu^2}{\sin^2(2\beta)} - 2\lambda_0 B_\mu v^2 \sin(2\beta) + \lambda_0^2 v^4 \sin^2(2\beta)} \\
m_\sigma^2 &= (\lambda_{56} + \lambda_{65})f^2 \equiv 2\lambda_0 f^2 K_\sigma
\end{aligned} \tag{3.3}$$

Since the quartic interaction, with coupling λ_0 , is produced when the heavy singlet state (σ) is integrated out, it is related to the fundamental parameters λ_{56} and λ_{65} via $\lambda_0 = \frac{2\lambda_{56}\lambda_{65}}{\lambda_{65} + \lambda_{56}}$. The factor K_σ represents a mixing between λ_{56} and λ_{65} , which is more simply expressed in terms of an overall factor.

There exist a number of theoretical constraints that can be placed on these parameters, primarily due to perturbativity requirements. The value of the mixing angle β is limited by two constraints, the first of which is the requirement that $\lambda_0 < 4\pi$, leading to an upper bound of

$$\tan \beta < \sqrt{\frac{m_{A_0}^2 8\pi v^2 + 4\sqrt{\pi v^2 m_{A_0}^2 (m_{A_0}^2 - m_{h_0}^2)(4\pi v^2 - m_{h_0}^2)}}{m_{h_0}^2 (m_{A_0}^2 - m_{h_0}^2 + 4\pi v^2)}} - 1. \quad (3.4)$$

A lower bound also exists, and is set by examining the radiatively-induced contributions to m_1 and m_2 in the model, which suggest that $\tan \beta \gtrsim 1$ [17]. Furthermore, there are limits on K_σ from requiring that $\lambda_{56/65}$ are real valued and $< 4\pi$, such that

$$\lambda_{56/65} = \frac{1}{2f^2} (m_\sigma^2 \pm \sqrt{m_\sigma^4 - 2f^2 m_\sigma^2 \lambda_0}) \longrightarrow 1 < K_\sigma < \frac{16\pi^2}{\lambda_0(8\pi - \lambda_0)} \quad (3.5)$$

The BLH model also contains two physical, real triplets, with charged fields ϕ^\pm and η^\pm that are relevant to the diphoton and $Z\gamma$ decay modes. While these fields obtain a contribution to their mass from the explicit symmetry breaking terms in the model, dependent on the parameter $m_4 \sim 10$ GeV, their masses are dominated by contributions from the Coleman-Weinberg potential involving gauge loops for ϕ^\pm and hypercharge boson loops for η^\pm . The dominant contribution to their masses are given by

$$\begin{aligned} M_{\phi^\pm}^2 &\approx \left[\kappa_G \frac{3}{32\pi^2} g_A^2 g_B^2 \left(1 - \frac{v^2}{2f^2} \frac{F^2}{f^2 + F^2} \right) \log \left(\frac{\Lambda^2}{M_{W'}^2} \right) \right] (f^2 + F^2) \\ M_{\eta^\pm}^2 &\approx \kappa_Y \frac{3}{16\pi^2} g'^2 \left(1 - \frac{v^2}{2f^2} \right) \Lambda^2, \end{aligned} \quad (3.6)$$

where $\Lambda \approx 4\pi f$ is the compositeness scale, and κ_G and κ_Y are taken as $\mathcal{O}(1)$ factors that account for the details of the cancellation of the gauge logarithmic, and hypercharge quadratic divergent loops, respectively, at the scale Λ . In our calculations, we take into account all contributions up to $O(v^2/f^2)$, including the subdominant explicit symmetry breaking mass terms [17], but do not show them here for brevity. The factors of g_A and g_B are the gauge couplings from $SU(2)_A$ and $SU(2)_B$, respectively, which will be discussed in further detail in section 3.2.

The scaling factors for the charged scalar interactions are given by

$$\begin{aligned} y_{h_0\eta^+\eta^-} &\approx -(c_\beta s_\alpha + c_\alpha s_\beta) \frac{v^2}{2f^2} \\ y_{H_0\eta^+\eta^-} &\approx -(c_\beta c_\alpha - s_\alpha s_\beta) \frac{v^2}{2f^2} \\ y_{h_0\phi^+\phi^-} &\approx -(c_\beta s_\alpha + c_\alpha s_\beta) \frac{v^2 F^2}{2f^2(f^2 + F^2)} \\ y_{H_0\phi^+\phi^-} &\approx -(c_\beta c_\alpha - s_\alpha s_\beta) \frac{v^2 F^2}{2f^2(f^2 + F^2)} \end{aligned} \quad (3.7)$$

$$\begin{aligned}
y_{h_0 H^+ H^-} &\approx \frac{v^2}{(768 f^2 m_{A_0}^2 \pi^2)} \left(-9 \kappa_G F^2 g_A^2 g_B^2 \log \left[\frac{\Lambda^2}{M_{W'}^2} \right] (c_\beta s_\alpha + c_\alpha s_\beta) \right. \\
&\quad \left. - 32 \kappa_S \lambda_0 m_\sigma^2 \log \left[\frac{\Lambda^2}{m_\sigma^2} \right] (3 c_\beta s_\alpha + 2 c_\alpha s_\beta) \right. \\
&\quad \left. + 128 \pi^2 c_\beta s_\beta (-6 f^2 \lambda_0 (c_\alpha c_\beta + s_\alpha s_\beta) + m_{A_0}^2 (c_\alpha c_\beta - s_\alpha s_\beta) (c_\beta^2 - s_\beta^2)) \right) \\
y_{H_0 H^+ H^-} &\approx \frac{v^2}{(768 f^2 m_{A_0}^2 \pi^2)} \left(9 \kappa_G F^2 g_A^2 g_B^2 \log \left[\frac{\Lambda^2}{M_{W'}^2} \right] (c_\beta c_\alpha - s_\alpha s_\beta) \right. \\
&\quad \left. + 32 \kappa_S \lambda_0 m_\sigma^2 \log \left[\frac{\Lambda^2}{m_\sigma^2} \right] (3 c_\beta s_\alpha + 2 c_\alpha s_\beta) (c_\beta^2 - s_\beta^2) \right. \\
&\quad \left. + 128 \pi^2 c_\beta s_\beta (6 f^2 \lambda_0 (-c_\alpha s_\beta + c_\alpha s_\beta) + m_{A_0}^2 (c_\alpha s_\beta + c_\alpha s_\beta) (c_\beta^2 - s_\beta^2)) \right)
\end{aligned}$$

where $c_\alpha = \cos \alpha$, $s_\alpha = \sin \alpha$, $c_\beta = \cos \beta$ and $s_\beta = \sin \beta$. The factor of κ_S is also taken as an $\mathcal{O}(1)$ factor that accounts for the details of the cancellation of the logarithmic divergence involving scalar loops. Here we have also neglected contributions from higher orders in the expansion of v/f , and terms proportional to the small explicit symmetry breaking parameters in the BLH model [17].

3.2 Gauge Sector

The gauge sector of the BLH model is expanded to $SU(2)_A \times SU(2)_B \times U(1)_X$, which breaks to $SU(2)_L \times U(1)_Y$. The expanded gauge sector results in the addition of three heavy gauge bosons, Z' and W'^{\pm} . However, because there is an additional global $SU(2)_A \times SU(2)_B$ symmetry that is gauged in the same way as the $SO(6)_A \times SO(6)_B$ and breaks to a diagonal $SU(2)$ at a scale $F > f$, the masses of the heavy gauge bosons are proportional to $\sqrt{f^2 + F^2}$ rather than simply f , as in other Little Higgs models. This results in the masses of the W' and Z' typically being larger than the masses of the heavy quarks, thereby evading constraints from fine-tuning and precision electroweak measurements [17].

The gauge couplings associated with $SU(2)_A \times SU(2)_B$, g_A and g_B , can be parameterized in a phenomenological fashion in terms of a mixing angle θ_g ($\tan \theta_g \equiv g_A/g_B$) and the $SU(2)_L$ gauge coupling, $g = g_A g_B / \sqrt{g_A^2 + g_B^2}$. Furthermore, the gauge coupling, g' , associated with the $U(1)_Y$ symmetry, and g can be parameterized as in the SM in terms of the fundamental charge, e , and the weak mixing angle, θ_w , such that $\sin \theta_w = g' / \sqrt{g^2 + g'^2}$, and $e = g \sin \theta_w$.

The masses of the gauge bosons in the BLH model are given by:

$$\begin{aligned}
M_{W'}^2 &= \frac{g^2 v^2}{4} \left(1 - \frac{v^2}{6 f^2} \left(1 + \frac{3}{2} \frac{f^2}{(f^2 + F^2)} (c_g^2 - s_g^2)^2 \right) \right) \\
M_Z^2 &= \frac{g^2 v^2}{4 c_w^2} \left(1 - \frac{v^2}{6 f^2} \left(1 + \frac{3}{2} \frac{f^2}{(f^2 + F^2)} (c_g^2 - s_g^2)^2 \right) \right) \\
M_{W'}^2 &= \frac{g^2}{4 c_g^2 s_g^2} (f^2 + F^2) - M_W^2 \\
M_{Z'}^2 &= M_{W'}^2 + \frac{g^2 s_w^2 v^4}{16 c_w^2 (f^2 + F^2)} (c_g^2 - s_g^2)^2
\end{aligned} \tag{3.8}$$

where $c_g = \cos \theta_g$ and $s_g = \sin \theta_g$. While both M_W^2 and M_Z^2 obtain corrections of $\mathcal{O}(v^4/f^2)$, which do not vanish as $F \rightarrow \infty$, the model retains custodial symmetry and such factors cancel out in their contribution to the ρ parameter. Additionally, corrections to the $Z\bar{f}f$ couplings are proportional to $v^2/(f^2 + F^2)$, and do vanish for $F \rightarrow \infty$ [17].

We use the experimental value of the fine structure constant, α_{EM} , to determine the value of e ($= \sqrt{\alpha_{EM}/4\pi}$), and calculate v and $\sin \theta_w$ from the experimental values of G_F and the pole mass of the Z boson, by exploiting the custodial symmetry relation, $\rho = 1$. Accounting for the contributions from the W and W' in the process $\mu \rightarrow e\bar{\nu}_e\nu_\mu$, gives an expression for the vev, v , in terms of the SM vev, such that

$$v = y_v v_{SM} = v_{SM} \left(1 + \frac{v_{SM}^2}{12f^2} \left(1 + \frac{f^2}{2(f^2 + F^2)} (3 + 12(c_g^2 - s_g^2)) \right) \right). \quad (3.9)$$

Combining this with the expression for the Z pole mass (\widehat{M}_Z), the weak mixing angle in the BLH model can be expressed as

$$\sin^2 \theta_w = \frac{1}{2} \left(1 - \sqrt{1 - \frac{e^2 v^2}{\widehat{M}_Z^2} \left(1 - \frac{v^2}{6f^2} \left(1 + \frac{3}{2} \frac{f^2}{f^2 + F^2} (s_g^2 - c_g^2) \right) \right)} \right). \quad (3.10)$$

The scaling factors important to the VBF and VH production modes, and to the diboson decay modes ($S_0 \rightarrow \gamma\gamma, VV^*$) are given by

$$\begin{aligned} y_{h_0 ZZ} &= (c_\beta s_\alpha + c_\alpha s_\beta) \left(1 - \frac{v^2}{6f^2} \left(1 + \frac{3}{4} \frac{f^2}{f^2 + F^2} (1 + c_g^4 - 6c_g^2 s_g^2 + s_g^4) \right) \right) \\ y_{h_0 WW} &= y_{h_0 ZZ} \\ y_{H_0 ZZ} &= \frac{(c_\beta c_\alpha - s_\alpha s_\beta)}{(c_\beta s_\alpha + c_\alpha s_\beta)} y_{h_0 ZZ} \\ y_{H_0 WW} &= \frac{(c_\beta c_\alpha - s_\alpha s_\beta)}{(c_\beta s_\alpha + c_\alpha s_\beta)} y_{h_0 ZZ} \\ y_{h_0 W'W'} &= -(c_\beta s_\alpha + c_\alpha s_\beta) \frac{c_g^2 s_g^2 v^2}{f^2 + F^2} \\ y_{H_0 W'W'} &= \frac{(c_\beta c_\alpha - s_\alpha s_\beta)}{(c_\beta s_\alpha + c_\alpha s_\beta)} y_{h_0 W'W'}. \end{aligned} \quad (3.11)$$

3.3 Fermion Sector

The Yukawa terms for the light fermions in the BLH model Lagrangian take the form of

$$\mathcal{L} = y_u f Q \Sigma U^c + y_d f Q (-2iT_R^2 \Sigma) D^c + h.c., \quad (3.12)$$

where T_R^2 is the second component of the triplet of $SU(2)_R$ generators corresponding to the $SO(4)_R$ subgroup of $SO(6)$, and performs the charge conjugation of the Higgs fields for interactions with the down-type quarks. This identifies the BLH model as a Type I 2HDM, with light fermion masses given by

$$M_f^2 = y_f^2 v^2 \sin^2 \beta \left(1 - \frac{v^2}{3f^2} + \dots \right). \quad (3.13)$$

and scaling factors of the form

$$\begin{aligned}
y_{h_0 f \bar{f}} &= \frac{c_\alpha}{s_\beta} - \frac{2v^2}{3f^2}(c_\beta s_\alpha + c_\alpha s_\beta) \\
y_{H_0 f \bar{f}} &= -\frac{s_\alpha}{s_\beta} - \frac{2v^2}{3f^2}(c_\beta c_\alpha - s_\alpha s_\beta) \\
y_{A_0 u \bar{u}} &= \frac{c_\beta}{s_\beta} + \frac{2v^2 c_\beta}{3f^2 s_\beta} \\
y_{A_0 d \bar{d}} &= -\frac{c_\beta}{s_\beta} - \frac{2v^2 c_\beta}{3f^2 s_\beta}
\end{aligned} \tag{3.14}$$

The BLH model also includes a number of heavy, vector-like quarks that act to protect the Higgs boson mass from developing quadratic divergences from the top quark loops. The Yukawa interactions for the heavy fermions, which includes the top quark, take the form:

$$\mathcal{L} = y_1 f Q_3 S \Sigma S U_3^c + y_2 f Q'_3 \Sigma U_3^c + y_2 f Q_3 \Sigma U_3'^c + h.c.. \tag{3.15}$$

These couplings can be simplified in terms of a reparameterization of y_2 and y_3 in terms of y_1 and two mixing angles, such that $y_2 = y_1 / \tan \theta_{12}$ and $y_3 = y_1 / \tan \theta_{13}$. The value of y_1 is then fixed through the measured top quark mass.

As we showed in [27], analytic methods for determining the mass eigenstates for the heavy quarks fail in the region where $|y_2 - y_3| \approx 0$, due to the degeneracy between the T and T_5 states. This can clearly be seen by observing a slice of the $(\tan \theta_{12}, \tan \theta_{13})$ parameter space, where $\tan \theta_{13} = 1 - \tan \theta_{12}$, as in Fig. 5. As a result, we use numerical diagonalization to determine the mass eigenstates of the heavy quarks, and thus their coupling to the h_0 , H_0 and A_0 states, for all values of $\tan \theta_{12}$ and $\tan \theta_{13}$. Therefore, we do not provide analytic solutions for the relevant scaling factors.

Since the vector-like quarks obtain contributions to their masses proportional to f , the lowest order contribution to their scaling factor is $\mathcal{O}(v/f)$, and their contribution to the loops in the $S_0 gg$ and $S_0 \gamma \gamma$ effective vertices drop off rapidly with increasing f . However, while the top quark is generated from the heavy quark Yukawa terms, it gets a mass proportional to v , and thus the dependence of the scaling factor for the top quark on β and α behaves at lowest order similar to the light up-type quarks. This dependence on β and α results in the most significant deviations from the SM to the fermion contributions to the loop interactions.

3.4 Parameter Survey

We use the following fixed values in our calculations:

$$\begin{aligned}
\alpha_{EM} &= 1/127.9 \\
G_F &= 0.0000116637 \text{ GeV}^{-2} \\
\widehat{M}_Z &= 91.1876 \text{ GeV} \\
M_t &= 172.5 \text{ GeV} \\
M_b &= 4.16 \text{ GeV}
\end{aligned}$$

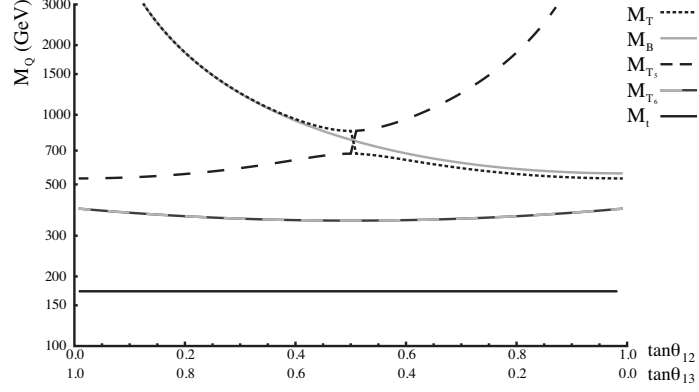


Figure 5. Slice of fermion mass plots, depending on mixing angles $\tan \theta_{12}$ and $\tan \theta_{13}$, corresponding to $(f = 1000 \text{ GeV}, \tan \beta = 3.35)$. The point at which the heaviest state switches from the T to T_5 is obvious.

$$\begin{aligned}
 M_\tau &= 1.77684 \text{ GeV} \\
 M_c &= 1.28 \text{ GeV} \\
 m_4 &= 30 \text{ GeV} \\
 m_5 &= 30 \text{ GeV} \\
 m_6 &= 30 \text{ GeV}
 \end{aligned}$$

Of note, the parameters $m_{4,5,6}$ are explicit symmetry breaking mass terms in the full BLH model scalar potential [17] that are small and provide a negligible contribution to the interactions examined.

To be thorough, we randomize all remaining parameters in the BLH model over the ranges:

$$\begin{aligned}
 m_{h_0} &\in (124, 126) \text{ GeV} \\
 m_{A_0} &\in (m_{h_0}, 700) \text{ GeV} \\
 f &\in (700, 3000) \text{ GeV} \\
 F &\in (f, 5000) \text{ GeV} \\
 \tan \beta &\in (1, \max(\tan \beta)) \text{ (see Eq. 3.4)} \\
 \tan \theta_g &\in (0, 5) \\
 \tan \theta_{12} &\in (0, 5) \\
 \tan \theta_{13} &\in (0, 5) \\
 K_\sigma &\in (1, \max(K_\sigma)) \text{ (see Eq. 3.5)} \\
 \kappa_G &\in (0, 5) \\
 \kappa_Y &\in (0, 5) \\
 \kappa_S &\in (0, 5)
 \end{aligned}$$

Since the mass of the observed resonance is not precisely known, and especially since the ZZ^* and $\gamma\gamma$ mass peak values in the ATLAS measurements are distinct, we allow the mass of the light Higgs boson to vary over a small range. All other values are calculated from this base set, as described in the preceding sections of this paper.

Table 1. Summary of published Higgs boson results from CMS. Note: The $\gamma\gamma$ result quoted uses the multi-variate analysis value, rather than the cut based analysis value.

Signal	Production	\mathcal{L}_7 (fb $^{-1}$)	\mathcal{L}_8 (fb $^{-1}$)	$\hat{\mu}$	m_h (GeV)
$\gamma\gamma$ [12]	Inclusive	5.1	19.6	$0.78^{+0.28}_{-0.26}$	125
ZZ^* [28]	Inclusive	5.1	19.6	$0.91^{+0.30}_{-0.24}$	125.8
ZZ^* [28]	VBF	5.1	19.6	$1.22^{+0.84}_{-0.57}$	125.8
WW^* [29]	ggF	4.9	19.5	0.76 ± 0.21	125
$b\bar{b}$ [30]	VH	5.0	12.1	$1.3^{+0.7}_{-0.6}$	125
$\tau^+\tau^-$ [31]	Inclusive	4.9	19.4	1.1 ± 0.4	125
$\tau^+\tau^-$ [31]	VBF	4.9	19.4	1.4 ± 0.6	125

Additionally, we separate our analysis into two groupings - a “general case”, where m_{A_0} varies up to 700 GeV, and a “near-degeneracy” case, where m_{A_0} can take a maximum value of 128 GeV.

4 Results

Both CMS and ATLAS have now published updated signal strengths for a given production mode and final state to account for the 7 TeV and 8 TeV data. We have calculated the expected value for these signal strength ratios in the BLH model for 60k parameter points. Specifically, we calculate:

$$\mu_{XX} = \frac{\mathcal{L}_7 \sum_i \sigma_{i,7}^{BLH} BR_{XX}^{BLH} + \mathcal{L}_8 \sum_i \sigma_{i,8}^{BLH} BR_{XX}^{BLH}}{\left(\mathcal{L}_7 \sum_i \sigma_{i,7}^{SM} BR_{XX}^{SM} + \mathcal{L}_8 \sum_i \sigma_{i,8}^{SM} BR_{XX}^{SM} \right) \Big|_{m_h = m_h^{exp}}}$$

where

$$BR_{XX} = \frac{\Gamma(S_0 \rightarrow XX)}{\sum_Y \Gamma(S_0 \rightarrow YY)} \quad (4.1)$$

The sum over the index i accounts for all contributing modes, including the A_0 and H_0 mediated production when $m_{A_0} - m_{h_0} < 2$ GeV and $m_{H_0} - m_{h_0} < 2$ GeV, respectively. Since the signal strengths from CMS and ATLAS are calculated based on the experimentally determined best fit mass, our μ values are normalized to the expected results for a SM Higgs boson with the mass given in the experimental study. Summaries of the published results from CMS and ATLAS can be found in Tables 1 and 2, respectively.

The ATLAS results present an unusual scenario where $\mu_{ZZ} \neq \mu_{WW}$, and consequently resulted in very poor agreement with most of the BLH model parameter space. In the BLH model, the relationship $\mu_{WW} \approx \mu_{ZZ}$ holds in both the general and the near-degenerate scenarios, with minor deviations arising due to the differences in the $V\bar{f}f$ couplings. It should be noted that statistically significant deviations from $\mu_{ZZ} \approx \mu_{WW}$ of the scale

Table 2. Summary of published Higgs boson results from ATLAS.

Signal	Production	\mathcal{L}_7 (fb $^{-1}$)	\mathcal{L}_8 (fb $^{-1}$)	$\hat{\mu}$	m_h (GeV)
$\gamma\gamma$ [14]	Inclusive	4.8	20.7	$1.65^{+0.34}_{-0.30}$	126.8
ZZ^* [32]	Inclusive	4.6	20.7	$1.7^{+0.5}_{-0.4}$	124.3
WW^* [33]	ggF+VBF	4.6	20.7	1.01 ± 0.31	125
WW^* [33]	VBF	4.6	20.7	1.66 ± 0.79	125
WW^* [33]	ggF	4.6	20.7	0.82 ± 0.36	125
$b\bar{b}$ [34]	VH	4.7	13.0	-0.4 ± 1.0	125
$\tau^+\tau^-$ [7]	Inclusive	4.6	13.0	0.7 ± 0.7	125

Table 3. Values of χ_{min}^2 in the general and near-degeneracy cases.

Near-degeneracy		General	
Experiment	χ_{min}^2	Experiment	χ_{min}^2
CMS	0.13	CMS	0.43
ATLAS	0.10	ATLAS	0.16

present in the ATLAS results would potentially rule out the entirety of the parameter space of the BLH model.

As a result of this, we have limited our χ^2 analysis to only include the $\gamma\gamma$ and WW^* results that have the lowest uncertainty for both ATLAS and CMS. Furthermore, this allows us to better showcase the two scenarios of the BLH model - in the general scenario, SM-like results favour the CMS results, while the ATLAS results favour the near-degeneracy scenario with $\mu_{\gamma\gamma} > 1$. For the other signal strength ratios, the BLH model parameter space allows for wide ranges of values, but favours SM-like results for the general case as f increases well above 1 TeV, as is apparent from Figures 6 through 12.

Figure 6 shows the dependence of $\mu_{\gamma\gamma}$ on the f parameter, where low values of f in the general scenario result in cancellations between the contributions from the new heavy particles and the contributions from the SM particles, resulting in $\mu_{\gamma\gamma} \rightarrow 0$. In the general scenario, the BLH model does produce SM-like results for the $\mu_{\gamma\gamma}$ signal strength ratio, which is in good agreement with the CMS results, for a value of $f \gtrsim 1300$ GeV. For this scenario, very little of the parameter space in the BLH model is in agreement with the ATLAS result of $\mu_{\gamma\gamma} > 1$, and this is the primary reason for the low density of $\Delta\chi^2 < 1$ points. However, in the near-degenerate case, the ATLAS results are in better agreement with the BLH model than the CMS results, over a larger range of parameter space, even down to $f \sim 700$ GeV. Likewise, Figure 7 shows the dependence of μ_{WW} on the f parameter, where a similar decrease in μ_{WW} as f decreases is apparent.

These conclusions are further supported by examining Fig. 8, where the right most plot also describes the regions of the parameter f corresponding to each point. It is evident that large values of f are favoured, as seen by comparing the CMS and ATLAS results to the f plot in the general case. The shift towards $\mu_{WW} \sim 1$ and $\mu_{\gamma\gamma} \sim 1.5$ for the ATLAS

results is also more apparent in the near-degeneracy plots.

However, these results are affected both by modifications to the production rate (predominantly ggF in both the $\gamma\gamma$ and WW^* final states), and by modifications to the branching ratios. The effect of the modification to the ggF production is examined in Figures 9 and 10, which plot the value of r_{hgg} versus μ_{WW} and $\mu_{\gamma\gamma}$, respectively. It is clear that the value of r_{hgg} is the dominant determining factor for the WW^* signal strength ratio, evidenced by the near-linear relationship for many of the parameter points in the general case. In the near-degeneracy scenario, $(\tan\beta)_{max} \sim 1$, and $\tan\alpha < 0$ is common. In such cases, the y_{hWW} coupling becomes small due to its $(c_\beta s_\alpha + c_\alpha s_\beta)$ dependence, where $c_\beta \approx s_\beta$, and s_α and c_α have opposite signs. The result is that many of the parameter points predict WW^* and $\gamma\gamma$ signal strengths much less than the SM predictions, regardless of a large ggF production rate.

Figure 11 includes information regarding the Higgs boson decays to fermions in the BLH model. For the general case, the BLH model predicts SM-like rates for $b\bar{b}$ decays. Since the $b\bar{b}$ mode requires associated production tagging to identify, the measured $b\bar{b}$ signal strength ratio looks very much like μ_{WW} in the near-degeneracy scenario, for values of $y_{hWW} \rightarrow 0$.

The $Z\gamma$ signal strength ratio in the BLH model is typically expected to be $\lesssim 1$, even for values of $\mu_{\gamma\gamma} > 1$. Except for a few outlier regions, this is generally true for all of the parameter space, as evident from Fig. 12. Thus, a statistically significant measured value of $\mu_{Z\gamma} > 1$ would be incompatible with the BLH model.

5 Summary

As a two Higgs doublet model, the Bestest Little Higgs model provides two possible scenarios: the general case in which only one Higgs state contributes to the observed Higgs boson results measured at ATLAS and CMS, and the near-degenerate case in which multiple Higgs states contribute to the observed results. We have shown that the general case provides large regions of parameter space that are in agreement with the CMS results ($\mu_{\gamma\gamma} \approx 1$ and $\mu_{WW} \approx \mu_{ZZ} \approx 1$), but little parameter space that is in agreement with the ATLAS results ($\mu_{\gamma\gamma} > 1$ and $\mu_{WW} \approx 1$). We have also shown that the unexpected ATLAS results can be accounted for within the near-degenerate scenario we explored, when we exclude the $\mu_{WW} \neq \mu_{ZZ} > 1$ result.

More accurate measurements, including the $b\bar{b}$, $\tau^+\tau^-$ and $Z\gamma$ final states, with higher luminosity will be crucial to determining the status of the BLH model.

Acknowledgments

The authors would like to thank Heather Logan, Thomas Grégoire, Stephen Godfrey, and Peter Winslow for guidance and assistance in this project. This research was supported in part by the Natural Sciences and Engineering Research Council of Canada.

References

- [1] G. Aad *et al.* [ATLAS Collaboration], “Observation of a new particle in the search for the Standard Model Higgs boson with the ATLAS detector at the LHC,” *Phys. Lett. B* **716**, 1 (2012) [arXiv:1207.7214 [hep-ex]].
- [2] S. Chatrchyan *et al.* [CMS Collaboration], “Observation of a new boson at a mass of 125 GeV with the CMS experiment at the LHC,” *Phys. Lett. B* **716**, 30 (2012) [arXiv:1207.7235 [hep-ex]].
- [3] [ATLAS Collaboration], “An update of combined measurements of the new Higgs-like boson with high mass resolution channels,” ATLAS-CONF-2012-170.
- [4] [CMS Collaboration], “Combination of standard model Higgs boson searches and measurements of the properties of the new boson with a mass near 125 GeV,” CMS-PAS-HIG-13-005.
- [5] K. Cheung, J. S. Lee and P. -Y. Tseng, “Higgs Precision (Higgcision) Era begins,” *JHEP* **1305**, 134 (2013) [arXiv:1302.3794 [hep-ph]].
- [6] [ATLAS Collaboration], “Observation and study of the Higgs boson candidate in the two photon decay channel with the ATLAS detector at the LHC,” ATLAS-CONF-2012-168.
- [7] [ATLAS Collaboration], “Search for the Standard Model Higgs boson in $H \rightarrow \tau\tau$ decays in proton-proton collisions with the ATLAS detector,” ATLAS-CONF-2012-160.
- [8] [ATLAS Collaboration], “Observation of an excess of events in the search for the Standard Model Higgs boson in the $H \rightarrow ZZ^* \rightarrow 4l$ channel with the ATLAS detector,” ATLAS-CONF-2012-169.
- [9] [CMS Collaboration], “Combination of standard model Higgs boson searches and measurements of the properties of the new boson with a mass near 125 GeV,” CMS-PAS-HIG-12-045.
- [10] [CMS Collaboration], “Updated results on the new boson discovered in the search for the standard model Higgs boson in the ZZ to 4 leptons channel in $p\bar{p}$ collisions at $\sqrt{s} = 7$ and 8 TeV,” CMS-PAS-HIG-12-041.
- [11] [CMS Collaboration], “Higgs to tau tau (SM) (HCP),” CMS-PAS-HIG-12-043.
- [12] [CMS Collaboration], “Updated measurements of the Higgs boson at 125 GeV in the two photon decay channel,” CMS-PAS-HIG-13-001.
- [13] [ATLAS Collaboration], “Combined coupling measurements of the Higgs-like boson with the ATLAS detector using up to 25 fb^{-1} of proton-proton collision data,” ATLAS-CONF-2013-034.
- [14] [ATLAS Collaboration], “Measurements of the properties of the Higgs-like boson in the two photon decay channel with the ATLAS detector using 25 fb^{-1} of proton-proton collision data,” ATLAS-CONF-2013-012.
- [15] J. Reuter and M. Tonini, “Can the 125 GeV Higgs be the Little Higgs?,” *JHEP* **1302**, 077 (2013) [arXiv:1212.5930 [hep-ph]].
- [16] X. -F. Han, L. Wang, J. M. Yang and J. Zhu, “Little Higgs theory confronted with the LHC Higgs data,” arXiv:1301.0090 [hep-ph].
- [17] M. Schmaltz, D. Stolarski and J. Thaler, “The Bestest Little Higgs,” *JHEP* **1009**, 018 (2010) [arXiv:1006.1356 [hep-ph]].

- [18] P. M. Ferreira, R. Santos, H. E. Haber and J. P. Silva, “Mass-degenerate Higgs bosons at 125 GeV in the Two-Higgs-Doublet Model,” *Phys. Rev. D* **87**, 055009 (2013) [arXiv:1211.3131 [hep-ph]].
- [19] J. F. Gunion, H. E. Haber, G. L. Kane and S. Dawson, “The Higgs Hunter’s Guide,” *Front. Phys.* **80**, 1 (2000).
- [20] R. Martinez, M. A. Perez and J. J. Toscano, “The Two Photon Decay Width Of The Higgs Boson In Left-Right Symmetric Theories,” *Phys. Rev. D* **40**, 1722 (1989).
- [21] T. Han, H. E. Logan, B. McElrath and L. -T. Wang, “Loop induced decays of the little Higgs: $H \rightarrow gg, \gamma\gamma$,” *Phys. Lett. B* **563**, 191 (2003) [Erratum-ibid. B **603**, 257 (2004)] [hep-ph/0302188].
- [22] S. Dittmaier *et al.* [LHC Higgs Cross Section Working Group Collaboration], “Handbook of LHC Higgs Cross Sections: 1. Inclusive Observables,” arXiv:1101.0593 [hep-ph].
- [23] W.-Y. Keung and W. Marciano, “Higgs Scalar Decays: $H \rightarrow W^\pm + X$,” *Phys. Rev. D* **30**, 248 (1984).
- [24] [CMS Collaboration], “Search for the Standard Model Higgs boson in the $H \rightarrow Z\gamma$ decay mode with pp collisions at $\sqrt{s} = 7$ and 8 TeV,” ATLAS-CONF-2013-009.
- [25] [CMS Collaboration], “Search for the standard model Higgs boson in the Z boson plus a photon channel in pp collisions at $\sqrt{s} = 7$ and 8 TeV,” CMS-PAS-HIG-13-006.
- [26] D. Eriksson, J. Rathsman and O. Stal, *Comput. Phys. Commun.* **181**, 189 (2010) [arXiv:0902.0851 [hep-ph]].
- [27] S. Godfrey, T. Gregoire, P. Kalyniak, T. A. W. Martin and K. Moats, “Exploring the heavy quark sector of the Bestest Little Higgs model at the LHC,” *JHEP* **1204**, 032 (2012) [arXiv:1201.1951 [hep-ph]].
- [28] [CMS Collaboration], “Properties of the Higgs-like boson in the decay $H \rightarrow ZZ \rightarrow 4l$ in pp collisions at $\sqrt{s} = 7$ and 8 TeV,” CMS-PAS-HIG-13-002.
- [29] [CMS Collaboration], “Evidence for a particle decaying to W^+W^- in the fully leptonic final state in a standard model Higgs boson search in pp collisions at the LHC,” CMS-PAS-HIG-13-003.
- [30] [CMS Collaboration], “Search for the standard model Higgs boson produced in association with W or Z bosons, and decaying to bottom quarks for HCP 2012,” CMS-PAS-HIG-12-044.
- [31] [CMS Collaboration], “Search for the Standard-Model Higgs boson decaying to tau pairs in proton-proton collisions at $\sqrt{s} = 7$ and 8 TeV,” CMS-PAS-HIG-13-004.
- [32] [ATLAS Collaboration], “Measurements of the properties of the Higgs-like boson in the four lepton decay channel with the ATLAS detector using 25 fb⁻¹ of proton-proton collision data,” ATLAS-CONF-2013-013.
- [33] [ATLAS Collaboration], “Measurements of the properties of the Higgs-like boson in the $WW^{(*)} \rightarrow \ell\nu\ell\nu$ decay channel with the ATLAS detector using 25 fb⁻¹ of proton-proton collision data,” ATLAS-CONF-2013-030.
- [34] [ATLAS Collaboration], “Coupling properties of the new Higgs-like boson observed with the ATLAS detector at the LHC,” ATLAS-CONF-2012-127.

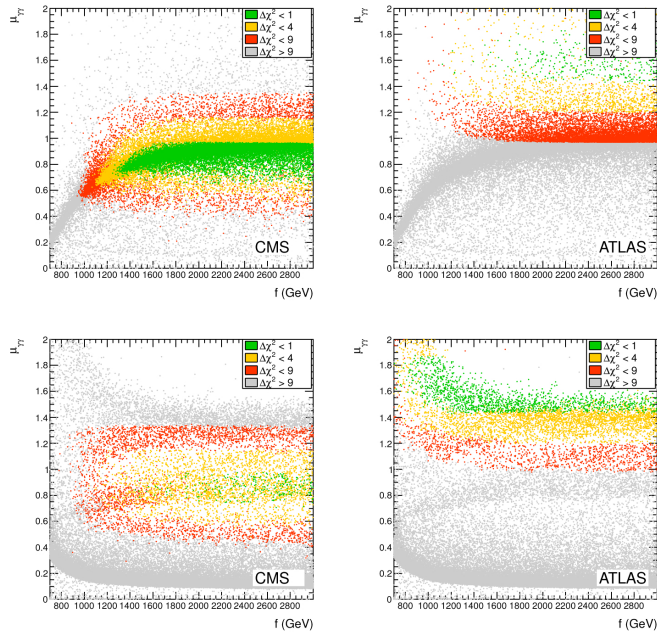


Figure 6. An examination of the dependence of $\mu_{\gamma\gamma}$ on the scale f shows good agreement for the CMS results in the general case for $f \gtrsim 1300$ GeV. Agreement between the ATLAS results and the near-degenerate case occurs for values as low as $f \sim 700$ GeV, while agreement with the CMS results in either scenario requires $f \gtrsim 1200$ GeV. The upper row of plots corresponds to the general case while the lower row corresponds to the near-degenerate case.

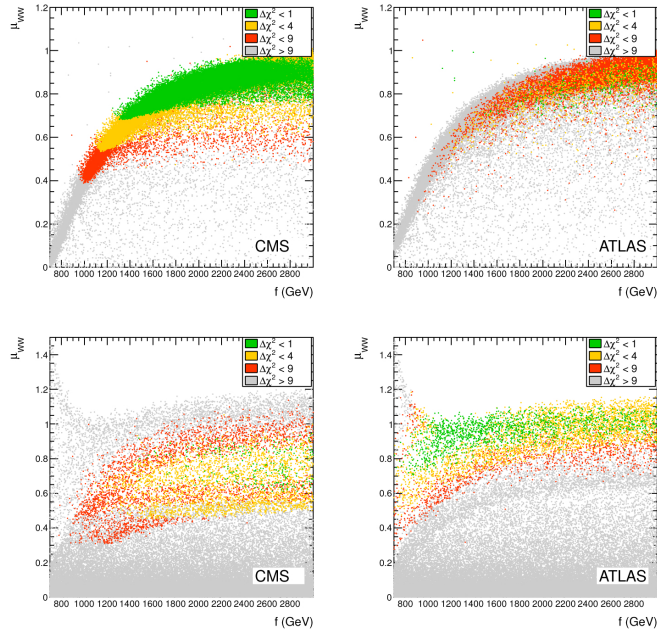


Figure 7. The leading contribution to $\mu_{\gamma\gamma}$ comes from loops involving the W boson and t quark, and so μ_{WW} drops similarly to $\mu_{\gamma\gamma}$ as $f \rightarrow 700$ GeV. The upper row of plots corresponds to the general case while the lower row corresponds to the near-degenerate case.

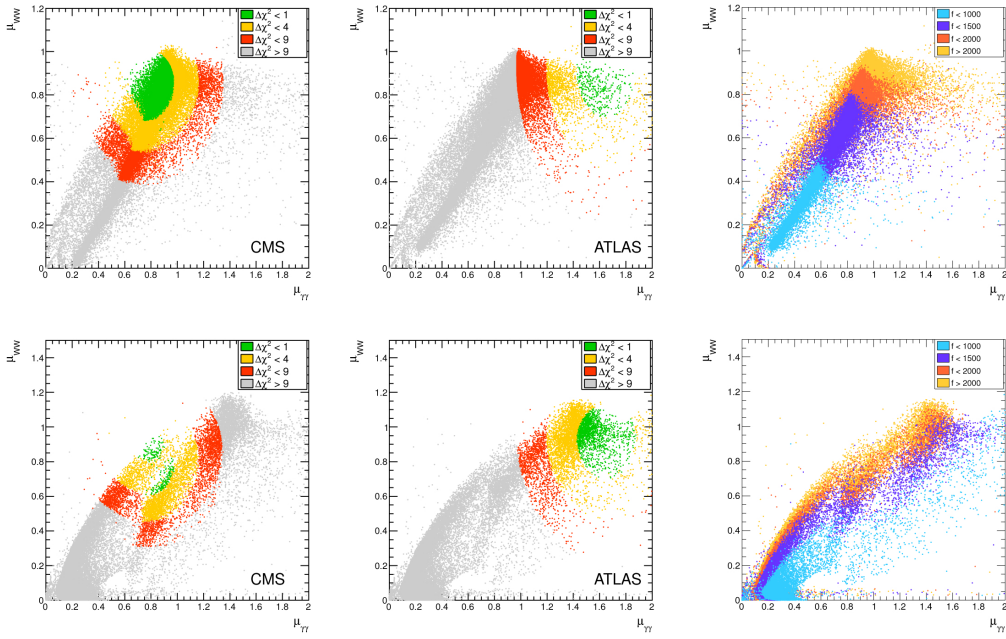


Figure 8. The two distinctive $\mu_{\gamma\gamma}$ values from ATLAS and CMS are apparent when plotting μ_{WW} versus $\mu_{\gamma\gamma}$. The regions of the parameter f are outlined in the plots on the right hand side. The upper row of plots corresponds to the general case while the lower row corresponds to the near-degenerate case.

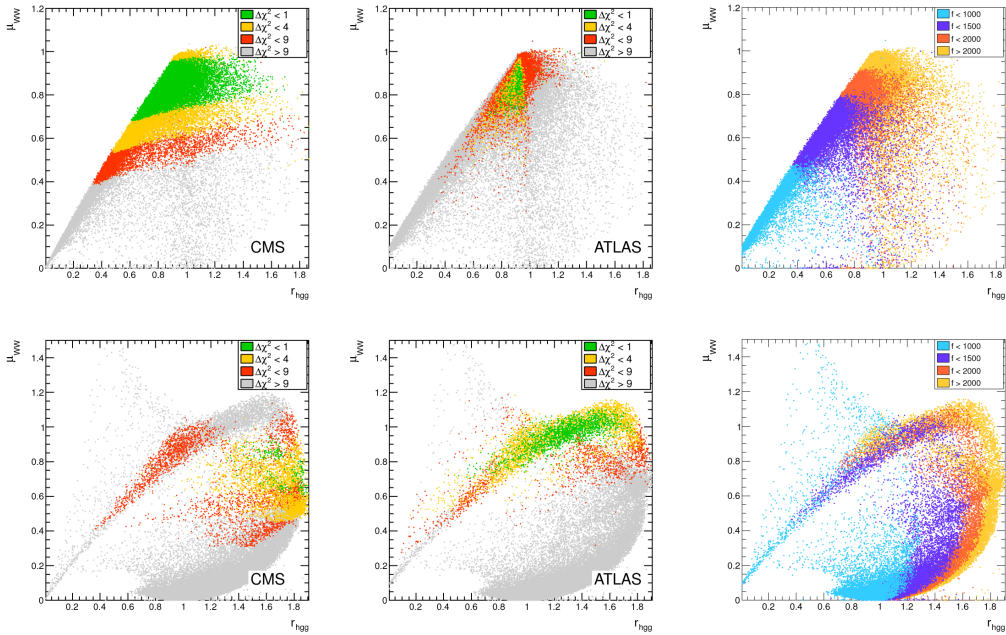


Figure 9. These plots examine how the μ_{WW} value depends on modifications to the ggF production rate. A large correlation is noticeable for the general case, but not for the near-degenerate case. The regions of the parameter f are outlined in the plots on the right hand side. The upper row of plots corresponds to the general case while the lower row corresponds to the near-degenerate case.

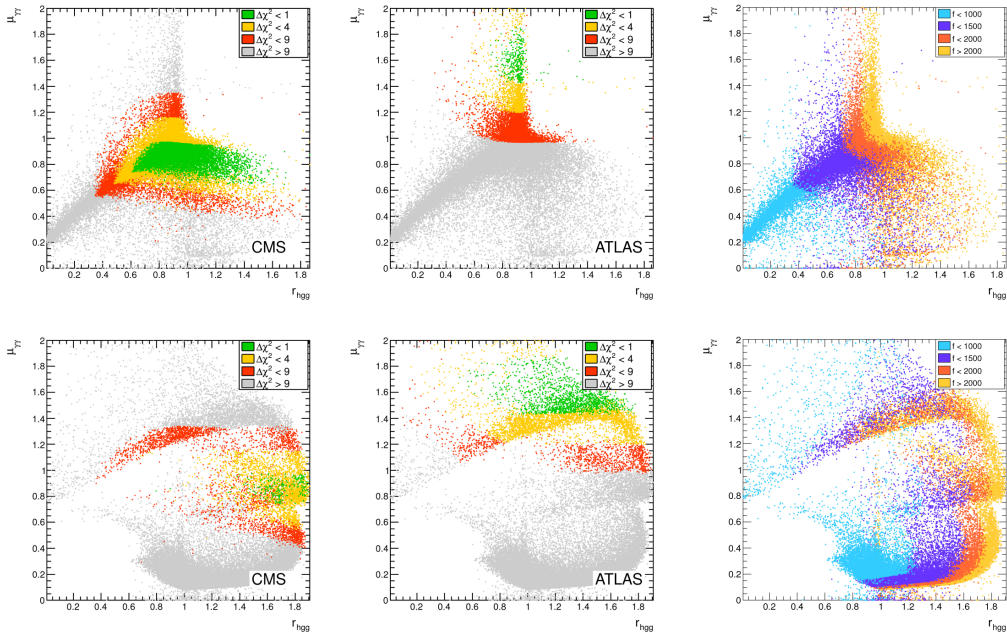


Figure 10. These plots examine how the $\mu_{\gamma\gamma}$ value depends on modifications to the ggF production rate. Large values of $r_{h\gamma\gamma}$ can result in large values of $\mu_{\gamma\gamma}$, even for smaller values of r_{hgg} . The regions of the parameter f are outlined in the plots on the right hand side. The upper row of plots corresponds to the general case while the lower row corresponds to near-degenerate case.

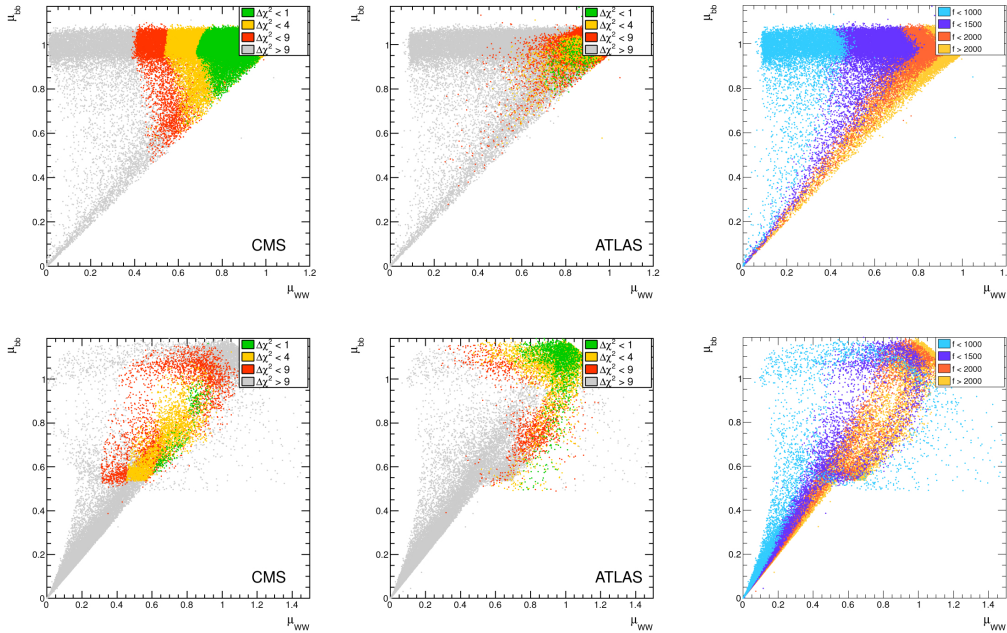


Figure 11. Values of $\mu_{WW} \sim 1$ similarly constrain the value of $\mu_{bb} \sim 1$ in the BLH model, which is a prediction that will be testable with more precise measurements of the $b\bar{b}$ final state. The regions of the parameter f are outlined in the plots on the right hand side. The upper row of plots corresponds to the general case while the lower row corresponds to the near-degenerate case.

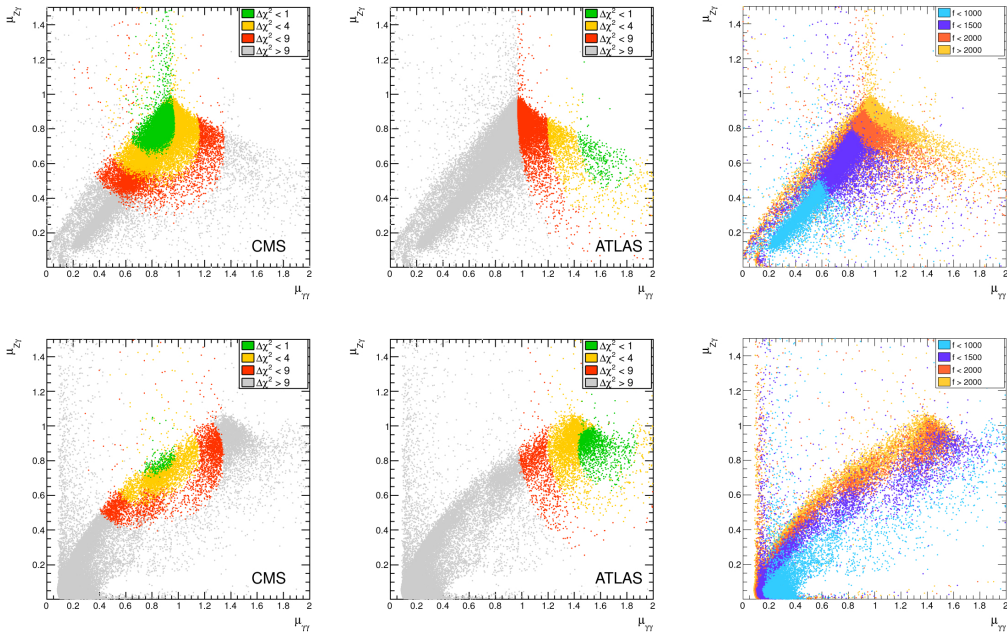


Figure 12. $\mu_{Z\gamma} \sim 1$ is consistent with both the ATLAS and CMS results, in both the general and near-degenerate cases. The regions of the parameter f are outlined in the plots on the right hand side. The upper row of plots corresponds to the general case while the lower row corresponds to the near-degenerate case.